

# Non-adiabatic holonomic quantum operations in continuous variable systems

Hao-Long Zhang,<sup>1</sup> Yi-Hao Kang,<sup>1</sup> Fan Wu,<sup>1</sup> Zhen-Biao Yang,<sup>1,\*</sup> and Shi-Biao Zheng<sup>1,†</sup>

<sup>1</sup>*Fujian Key Laboratory of Quantum Information and Quantum Optics,  
College of Physics and Information Engineering,  
Fuzhou University, Fuzhou, Fujian 350116, China*

(Dated: May 22, 2024)

Quantum operations by utilizing the underlying geometric phases produced in physical systems are favoured due to its potential robustness. When a system in a non-degenerate eigenstate undergoes an adiabatically cyclic evolution dominated by its Hamiltonian, it will get a geometric phase, referred to as the Berry Phase. While a non-adiabatically cyclic evolution produces an Aharonov-Anandan geometric phase. The two types of Abelian geometric phases are extended to the non-Abelian cases, where the phase factors become matrix-valued and the transformations associated with different loops are non-commutable. Abelian and non-Abelian (holonomic) operations are prevalent in discrete variable systems, whose limited (say, two) energy levels, form the qubit. While their developments in continuous systems have also been investigated, mainly due to that, bosonic modes (in, such as, cat states) with large Hilbert spaces, provide potential advantages in fault-tolerant quantum computation. Here we propose a feasible scheme to realize non-adiabatic holonomic quantum logic operations in continuous variable systems with cat codes. We construct arbitrary single-qubit (two-qubit) gates with the combination of single- and two-photon drivings applied to a Kerr Parametric Oscillator (KPO) (the coupled KPOs). Our scheme relaxes the requirements of the previously proposed adiabatic holonomic protocol dependent on long operation time, and the non-adiabatic Abelian ones relying on a slight cat size or an ancilla qutrit.

PACS numbers: 03.65.Vf, 03.67.-a, 42.50.Pq

Keywords: Cat qubit, Continuous variable systems, non-Abelian

## I. INTRODUCTION

The concept of geometric phases was first proposed by Berry [1], who discovered that a quantum system in a non-degenerate eigenstate of an adiabatically and cyclically changed Hamiltonian will pick up a path-dependent phase, in addition to the dynamical one. This phase only depends on the global geometric feature of the loop traversed in parameter space, and hence is insensitive to fluctuations of the control parameters [2]. This feature is favorable for implementation of quantum logic gates theoretically [3, 4] and experimentally [5, 6]. However, the long operation time imposed by the adiabatic condition represents a disadvantage in view of decoherence [7, 8]. To overcome this problem, one treatment is to design driving algorithms or optimized techniques to speed up this process [9–13]. The other is non-adiabatic geometric quantum computation protocols, which are based on the non-adiabatic geometric phase proposed by Aharonov and Anandan [14]. These protocols have been proposed [15, 16] and experimentally demonstrated [17–25].

These geometric phases are Abelian as the phase factors associated with distinct loops are commutable. Non-Abelian geometric phase offers an alternative strategy for realizing noise-resilient logic gates. Such phases were first discovered in a quantum system whose Hamiltonian has generate eigenstates [26]. An adiabatically and cycli-

cally change of such a Hamiltonian will result in a matrix-valued phase factor. Quantum logic operations based on such non-Abelian phases are referred to as adiabatic Holonomic gates [27, 28]. Despite fundamental interest, the practicality of such gates is also challenged by the adiabatic condition, resulting in limited experimental realization [29, 30]. To remove this restriction, non-adiabatic holonomic gates have been proposed [31–36] and further improved [37–50]. So far, such gates have been experimentally implemented in different systems, including superconducting circuits [11, 51–58], nuclear magnetic resonance [59–61], nitrogen-vacancy centers [62–67], trapped ions [68].

The above protocols focus on discrete-variable-encoded qubits. During the past decade, increasing efforts in quantum error correction [49, 69–71] have been paid to continuous-variable encoding schemes, where the logic qubits are encoded in some continuous-variable of bosonic modes, e.g., amplitudes of light fields [71–78]. Thanks to the infinite-dimensional Hilbert space of bosonic modes, such encoding schemes are hardware efficient in contrast to surface code [49, 50, 79–82]. Among various continuous-variable-encoded qubits, the cat qubit is particularly intriguing, whose codewords are encoded in two cat states with opposite parities [83–92]. The most remarkable feature of such qubits is noise bias. In other words, with the increase of cat size the bit flip error is exponentially suppressed, while the phase flip error only linearly grows [83, 86, 93, 94]. More importantly, such an encoding scheme may circumvent the no-go theorem, which states that it is impossible to realize a universal set of logic gates in a fault-tolerant manner with con-

\* zbyang@fzu.edu.cn

† t96034@fzu.edu.cn

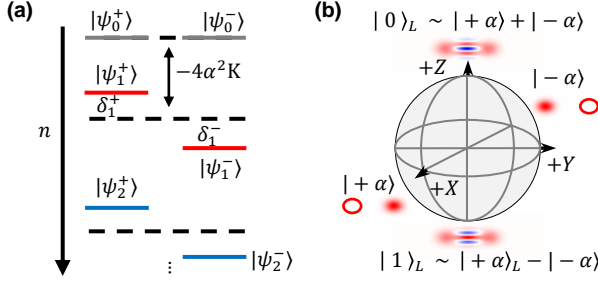


FIG. 1. (a) Energy spectra of the continuous variable KPO. The eigenstates are divided into even and odd parities.  $\delta_n$  is the energy gap between the  $n$ -th pair of eigenstates. (b) Bloch sphere of the cat qubit and the corresponding Wigner function representations (shown for  $|\alpha|^2 = 2.34$ ). The two cat states act as the logical qubits and are encoded as  $|0\rangle_L$  and  $|1\rangle_L$ .

ventional encoding schemes [93]. Up to now, dynamical logic gates for cat qubits have been proposed [83, 85–87, 93, 95, 96] and demonstrated [97, 98]. Recently, adiabatic holonomic gates based on the encoding schemes with coherent states or cat states have been proposed [88], but these gates suffer from long operation time. In addition, non-adiabatic geometric gates for such qubits have been presented, but which are restricted to a small cat size [99] or require an ancilla qutrit [100]. We here present a scheme for realizing non-adiabatic holonomic gates with cat qubits. In addition to the non-Abelian character, the gate can overcome these problems in Refs. [99, 100]. In our scheme, the codewords of the qubit is encoded in two degenerate eigenstates of a Kerr Parametric Oscillator (KPO), the even and odd cat states. By coupling these two cat states to another eigenstate with a two-photon drive and a one-photon drive, a non-adiabatic holonomic gate for the cat qubit can be realized. We further investigate the implementation of holonomic gates between two cat qubits.

## II. SPECTRUM OF THE KPO SYSTEM

We consider a KPO system, for which the cat qubit spanned by the coherent states can be confined within the subspace  $\{|\pm\alpha\rangle\}$  by the Kerr non-linearity and the two-photon drive. The Hamiltonian in the frame rotating at half of the oscillator frequency is

$$\hat{H}_{\text{KPO}} = -K\hat{a}^{\dagger 2}\hat{a}^2 + P(\hat{a}^2 + \hat{a}^{\dagger 2}), \quad (1)$$

where  $\hat{a}$  and  $\hat{a}^\dagger$  are the annihilation and creation operators for the KPO,  $K$  is Kerr nonlinearity, and  $P$  is the amplitude for the drive. This Hamiltonian can be rewritten as  $\hat{H}_{\text{KPO}} = -K(\hat{a}^{\dagger 2} - \alpha^{*2})(\hat{a}^2 - \alpha^2) + P/K$ , where  $\alpha = \sqrt{P/K}$ , clearly showing that the two coherent states  $|\pm\alpha\rangle$  are eigenstates of  $\hat{H}_{\text{KPO}}$ .

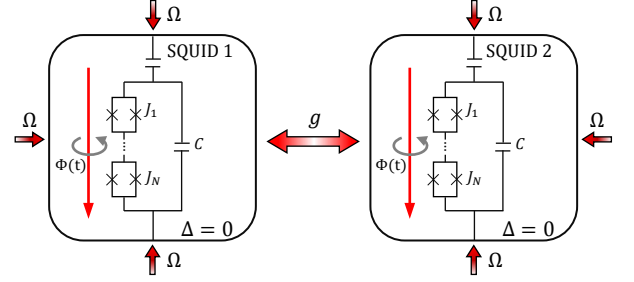


FIG. 2. Circuit diagram of the coupled KPOs. The KPO in each node is controlled by a high-frequency external flux  $\Phi$ . The double-headed arrow denotes the coupling between two KPOs with the coupling strength  $g$  and the single-headed arrows denote the external drives with strength  $\Omega$ .

The energy spectra of the KPO are shown in Fig. 1(a), where the eigenstates  $|\psi_n^\pm\rangle$  are spanned with two different parity; wherein the even/odd cat states  $|\psi_0^\pm\rangle = \mathcal{N}_0^\pm(|\alpha\rangle \pm |-\alpha\rangle)$  construct the degenerate eigenstate space, which can be exploited to be a couple of computational bases [Fig. 1(b)]. The eigenenergies are figured out approximately by the shifted Fock basis picture transformation [83] as

$$E_n^\pm = -4nK|\alpha^2| + \delta_n^\pm, \quad (2)$$

where  $\pm$  labels the parity of eigenstates,  $n = 1, 2, \dots$  and  $\delta_n$  exponentially decreases as  $\alpha$  goes up. When  $\alpha$  is large, the eigenstates can be described by the shifted Fock states  $|\psi_n^\pm\rangle = \mathcal{N}_n^\pm[\hat{D}(\alpha) \pm (-1)^n \hat{D}(-\alpha)]|n\rangle$ .

To engineer the KPO system, we may consider the model as reported in [101]. As shown in Fig. 2, each node of the coupled KPOs consisting of a large capacitor and  $N$  junctions are induced by a high-frequency magnetic flux to construct the superconducting quantum interference device (SQUID) array.

## III. SINGLE-QUBIT GATES

In the following, we show how to perform single-qubit non-adiabatic holonomic operations in the KPO system. As shown in Fig. 3(a), the first to realize such operations is to construct a three-level configuration (see Appendix A), such as  $\Lambda$  [32],  $V$  [63] and  $\Xi$  [56] forms. Here we choose  $\{|\psi_0^+\rangle, |\psi_0^-\rangle, |\psi_1^+\rangle\}$  as the bases to act as the computational subspace  $\{|0\rangle_L, |1\rangle_L, |2\rangle_L\}$  for the non-adiabatic holonomic operation. Due to the potential leakage to the other states, we also consider  $|\psi_1^-\rangle$  as the leaked state which is labeled  $|3\rangle_L$ .

In our scheme, we consider  $V$  configuration to perform the non-adiabatic holonomic dynamics. We use two-photon and single-photon drives with different amplitudes  $\Omega_{c0}/2, \Omega_{c1}/2$  but with same frequencies  $\omega$ . The

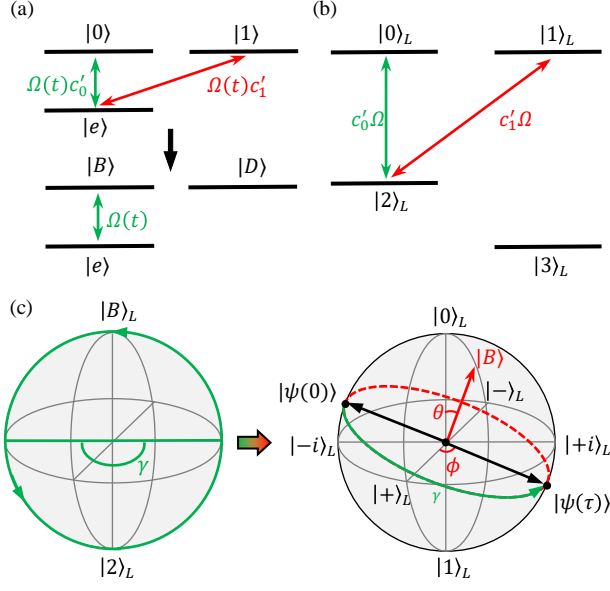


FIG. 3. (a) The mechanism of non-adiabatic holonomic quantum operations in a  $V$  configuration. This interaction can be equivalent to the oscillation between the bright state  $|B\rangle = -a|0\rangle + b|1\rangle$  and  $|e\rangle$ . (b) The mechanism of the non-adiabatic holonomic evolution in the continuous variable KPO system under the single-photon and two-photon drives. The drive amplitudes here are chosen as constant for convenience. (c) Dynamics of non-adiabatic holonomic interaction in a cyclic evolution. This process can be equivalent to the rotation along axis of the bright state  $|B\rangle$  with angle  $\gamma$ .

system can be described as below:

$$\begin{aligned}\hat{H}_{\text{Single}} &= \hat{H}_{\text{KPO}} + \hat{H}_t + \hat{H}_s, \\ \hat{H}_t &= \frac{\Omega}{2} \left[ c_0 e^{-i(\omega t + \xi)} \frac{\hat{a}^2}{2} + \text{H.c.} \right], \\ \hat{H}_s &= \frac{\Omega}{2} \left[ c_1 e^{-i(\omega t + \xi)} \hat{a} + \text{H.c.} \right],\end{aligned}\quad (3)$$

where  $\hat{H}_t$  and  $\hat{H}_s$  represent two-photon and single-photon drives, respectively. We let  $\omega = (E_1^+ - E_0)/\hbar$ . Under the condition  $\Omega \ll (E_j - E_0)/\hbar$  ( $j = 3, 4, 5, \dots$ ), the transitions with higher excited states can be ignored due to the rotating wave approximation. Owing to parity selectivity, the single-photon drive only couples the transition  $|1\rangle_L \leftrightarrow |2\rangle_L$ , while the two-photon drive only couples the transition  $|0\rangle_L \leftrightarrow |2\rangle_L$ . In the interaction picture with respect to  $H_0$ , the Hamiltonian can be rewritten as:

$$\hat{H}'_{\text{Single}} = \frac{\Omega}{2} (c'_0 e^{-i\xi} |2\rangle_L \langle 1| + c'_1 e^{-i\xi} |2\rangle_L \langle 0| + \text{H.c.}), \quad (4)$$

where  $c'_0 = c_0 \langle 1| a |2\rangle_L$  and  $c'_1 = c_1 \langle 0| a^2 |2\rangle_L/2$ . We control  $|c'_0|^2 + |c'_1|^2 = 1$ . The Hamiltonian of Eq. (4) processes a dark state  $|D\rangle = -c'_0|0\rangle_L + c'_1|1\rangle_L$ , which remains steady during the evolution, while keeping the bright state  $|B\rangle = c'_1|0\rangle_L + c'_0|1\rangle_L$  evolving through the oscillation mediated with the excited state  $|2\rangle_L$ .

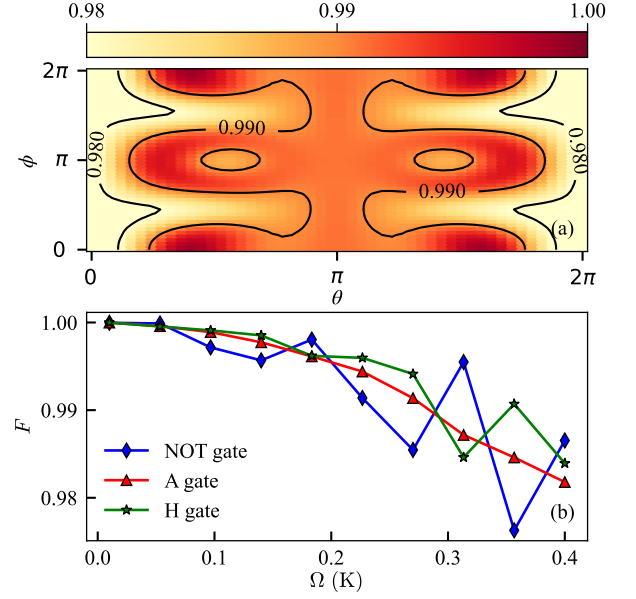


FIG. 4. Simulation results of the single-qubit gates. (a) The gate fidelity, defined in Eq. (6), versus the parameters  $(\theta, \phi)$  within  $[0, 2\pi]$  for  $\Omega = 0.25\text{K}$  and  $\gamma = 0$ . (b) The gate fidelity of the NOT, A and H gates as a function of  $\Omega/\text{K}$ , with  $(|\alpha|^2, T_g) = (2.3, 2\pi/\Omega)$ . The parameters  $(\theta, \phi)$  for the simulated NOT, A and H gates are chosen as  $(3\pi/2, 0)$ ,  $(3\pi/2, \pi/4)$  and  $(7\pi/4, 0)$ , respectively.

After a cyclic evolution with the driving duration  $T_g$ , the whole system turns back to the computational subspace and obtains a relative phase  $\gamma = \int_0^{T_g} \Omega/2 dt = \pi + \xi$ . This process can be characterized by the transformation:  $\hat{U}_{\text{Single}} = |D\rangle \langle D| + e^{i\gamma} |B\rangle \langle B|$ . This transformation is a universal operation, which can be regarded as a rotation by an angle  $\gamma$  around the axis of  $|B\rangle$  on the Bloch sphere, as shown in Fig. 3 (c). Provided that  $\xi = 0$ ,  $c'_0 = \sin(\theta/2)e^{-i\phi}$  and  $c'_1 = \cos(\theta/2)$ , this corresponds to  $\mathbf{n} \cdot \boldsymbol{\sigma}$ , where  $\mathbf{n} = (\sin \theta \cos \phi, \sin \theta \sin \phi, \cos \theta)$  and  $\boldsymbol{\sigma} = (\hat{\sigma}_x, \hat{\sigma}_y, \hat{\sigma}_z)$  (see Appendix A). The evolution operator for the subspace  $\{|0\rangle_L, |1\rangle_L\}$  is:

$$\hat{U}_{\text{Single}}(\theta, \phi) = \begin{pmatrix} \cos \theta & e^{-i\phi} \sin \theta \\ e^{i\phi} \sin \theta & -\cos \theta \end{pmatrix}. \quad (5)$$

By controlling  $\xi$ ,  $c_0$  and  $c_1$ , we can realize the universal single-qubit gates with different parameter  $(\gamma, \phi, \theta)$ . Since the parallel-transport condition  ${}_L \langle k | \hat{H}'_{\text{Single}} | l \rangle_L = 0$  ( $k, l = 0, 1$ ) is satisfied, this evolution is purely geometric. What's more, it is also a non-Abelian operation and can be verified with the choices of  $(\gamma, \theta, \phi) = \{(0, 0, 0), (0, 0, \pi/2)\}$ , which correspond to  $\hat{\sigma}_z$  and  $\hat{\sigma}_x$  operations, respectively. We perform these two operations on arbitrary quantum states in a different order and test to verify that the results of final states are promising.

We now turn to the discussion of the gate operation time, which is limited by the Kerr nonlinearity  $K$ . In general, a large  $K$  is favorable. As shown below, the gate

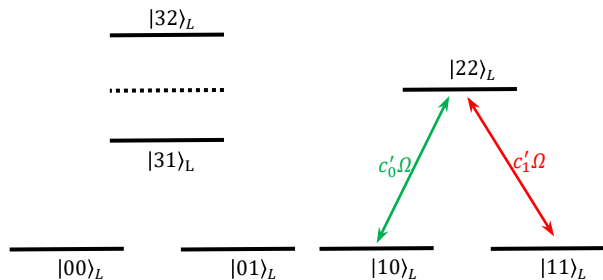


FIG. 5. Partial level construction of the two-qubit KPO system,  $\{|00\rangle, |01\rangle, |10\rangle, |11\rangle\}$  are degenerate ground states and  $|22\rangle$  is the excited state. Here we consider  $\{|31\rangle, |32\rangle\}$  as leakage states due to level leakage during gate operation process.

operation time is proportional to  $K^{-1}$  [96]. To verify the above discussion, we numerically calculate the gate fidelity through the method of the quantum process tomography, which is defined as [56, 102]

$$F = \text{tr}(\chi_{\text{id}}\chi_{\text{num}}), \quad (6)$$

where  $\chi_{\text{id}}$  is the ideal process matrix and  $\chi_{\text{num}}$  is the process matrix obtained by the numerical simulation. The parameters are set as  $\Omega = 0.25K$  and  $|\alpha|^2 = 2.34$ .

As shown in Fig. 4(a), the gate operations with partial angles have relatively low fidelities, which is due to incomplete gate operations and the leakage to the higher excited states. This error can be reduced to the minimum through the control of  $c_0$  and  $c_1$ . Actually, arbitrary non-adiabatic holonomic single-qubit gates for parameters  $(\theta, \phi)$  can be achieved with high fidelity as long as the Rabi frequency of the drive  $\Omega$  is controlled appropriately. The gate fidelity goes up as  $\Omega$  decreases, but the corresponding time  $T_g = 2\pi/\Omega$  will be extended. Notice that  $\Omega$  is still required to be optimized so as to completely avoid the coupling of the computational space to the higher excited states.

If we choose small  $\alpha$ , all the energy gaps are too small to cause leakage to higher excited states but not only the excited state  $|3\rangle_L$ . When  $\alpha$  is too large, the leakage to  $|3\rangle_L$  will be intensified, scrambling evolution of the non-adiabatic holonomic process. Maybe this limit can be overcome through derivative-based corrections [83].

To avoid the effect of leakage, we assume  $\alpha^2$  is large enough so that we can choose an appropriate  $\Omega$  to perform non-adiabatic holonomic evolution. Similar to those reported in Ref. [63], we choose  $(\theta, \phi)$  as  $(3\pi/2, 0)$ ,  $(3\pi/2, \pi/4)$ , and  $(7\pi/4, 0)$ , which correspond to NOT, A, and H gates, respectively. These gates constitute a complete set of single-qubit operations. The gate fidelities with  $\Omega$  are shown in Fig. 4(b). It can be found that, the fidelities of these gate become higher as the amplitude of drive increases, and the operation time decreases as the Kerr nonlinearity increases.

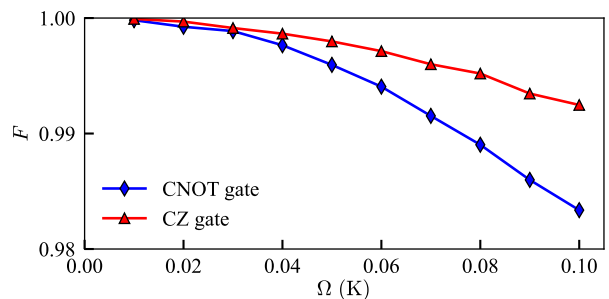


FIG. 6. Simulated gate fidelities, defined in Eq. (6), of the CNOT and CZ gates versus  $\Omega/K$ , with  $(|\alpha|^2, T_g) = (2.3, 2\pi/\Omega)$ . The parameters  $(\theta, \phi)$  for the simulated CNOT and CZ gates are chosen as  $(3\pi/2, 0)$  and  $(0, 0)$ , respectively.

#### IV. TWO-QUBIT GATE

To realize a two-qubit non-adiabatic holonomic gate, we also need to construct a  $V$  model, whose realization depends on the control-qubit: only the control-qubit is in  $|1\rangle_L$  such that the target-qubit flips through the holonomic dynamics otherwise remains steady. The Hamiltonian can be written as follows:

$$\hat{H} = |1\rangle_L \langle 1| \otimes \hat{H}'_{\text{Single}} + |0\rangle_L \langle 0| \otimes \hat{I}, \quad (7)$$

where  $\hat{I}$  is identity operator of the cat qubit, and  $\hat{H}'_{\text{Single}}$  is the single-qubit Hamiltonian in Eq. (4). Here we induce two non-energy-conserving couplings to realize the two-qubit gate.

As shown in Fig. 5, the two drives couple  $|10\rangle_L$  and  $|11\rangle_L$  to  $|22\rangle_L$  but not cause the coupling of  $|00\rangle_L$  and  $|01\rangle_L$  to any other states ( $|jk\rangle_L \equiv |j\rangle_L \otimes |k\rangle_L$ , the 1st and 2nd vectors represent the control qubit and the target qubit), due to parity selectivity and large detuning. The Hamiltonian is:

$$\hat{H}_{\text{Two}} = \hat{H}_{\text{KPO},2} + \hat{H}_{t,2} + \hat{H}_{s,2}, \quad (8)$$

with

$$\begin{aligned} \hat{H}_{\text{KPO},2} &= \hat{H}_{\text{KPO}} \otimes \hat{I} + \hat{I} \otimes \hat{H}_{\text{KPO}}, \\ \hat{H}_{t,2} &= \frac{\Omega}{2} \left[ c_0 e^{-i(\omega_{22}t + \xi)} \hat{a} \otimes \hat{b}^2 + \text{H.c.} \right], \\ \hat{H}_{s,2} &= \frac{\Omega}{2} \left[ c_1 e^{-i(\omega_{22}t + \xi)} \hat{a} \otimes \hat{b} + \text{H.c.} \right], \end{aligned} \quad (9)$$

where  $\hat{H}_{\text{KPO},2}$  describes the two-qubit KPO system,  $\hat{a}$  and  $\hat{b}$  are the annihilation operators for the control-KPO and the controlled-KPO, respectively,  $\hat{H}_{t,2}$  represents two-photon coupling for the  $|10\rangle \leftrightarrow |22\rangle$  transition and  $\hat{H}_{s,2}$  is single-photon coupling for the  $|11\rangle \leftrightarrow |22\rangle$  transition. Let  $\xi = 0$ . After a cyclic evolution, the corresponding evolution operator of the cat qubits is:

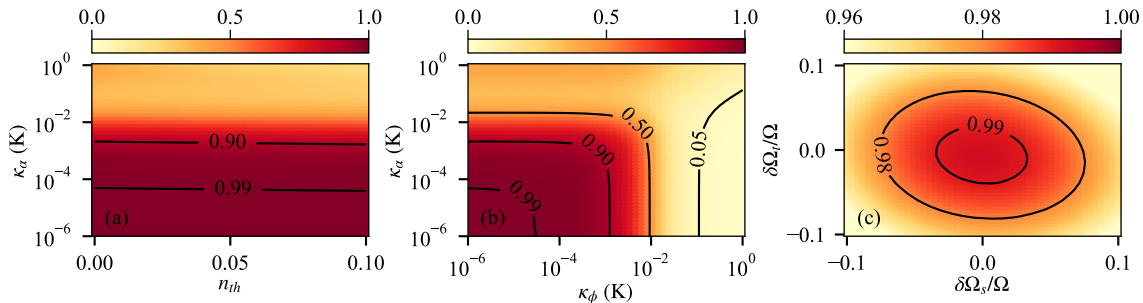


FIG. 7. The simulated results for the fidelity, defined in Eq. (6), of the NOT gate under the influences of noises, for  $\Omega = 0.23\text{K}$ . (a) The gate fidelity as a function of rate of the rescaled single-photon loss  $\kappa_\alpha/\text{K}$  and the number of thermal photons  $n_{th}$ . (b) The gate fidelity as a function of the rescaled single-photon loss rate  $\kappa_\alpha/\text{K}$  and the rescaled dephasing rate  $\kappa_\phi/\text{K}$ . (c) The gate fidelity as a function of the rescaled amplitude fluctuation for the single-photon drive,  $\delta\Omega_s/\Omega$ , and for the two-photon drive,  $\delta\Omega_t/\Omega$ .

$$\hat{U}_{\text{Two}}(\theta, \phi) = \begin{pmatrix} 1 & 0 & 0 & 0 \\ 0 & 1 & 0 & 0 \\ 0 & 0 & \cos\theta & e^{-i\phi}\sin\theta \\ 0 & 0 & e^{i\phi}\sin\theta & -\cos\theta \end{pmatrix}. \quad (10)$$

We can realize the CNOT gate with the choice of  $(\phi, \theta) = (0, 3\pi/2)$  and the CZ gate with the choice of  $(\phi, \theta) = (0, 0)$ . To verify this method, we perform the numerical simulation. As can be seen from Fig. 6, the CNOT gate with fidelity above 99% can be achieved for  $\Omega < 0.08\text{K}$ , while the case for the CZ gate is better, with the main error due to the leakage out of the non-adiabatic holonomic state evolution subspace. In fact, the constructed gate operation can be extended to non-adiabatic non-Abelian arbitrary two-qubit gate operation.

## V. ANALYSIS OF DECOHERENCE AND LEAKAGE

In this section, we study the impact of decoherence process and leakage to the higher excited states. The full dynamics of the driven KPO can be described by the Markov master equation [103]:

$$\begin{aligned} \frac{d\hat{\rho}}{dt} = & -i[\hat{H}_{\text{Single}}, \hat{\rho}] + \kappa_\alpha(1 + n_{th})D[\hat{a}]\hat{\rho} \\ & + \kappa_\alpha n_{th}D[\hat{a}^\dagger]\hat{\rho} + \kappa_\phi D[\hat{a}^\dagger\hat{a}]\hat{\rho}, \end{aligned} \quad (11)$$

where  $\kappa_\alpha$  is the single-photon loss rate,  $n_{th}$  is the number of thermal photons and  $\kappa_\phi$  is the rate of pure dephasing. We analyze it from two aspects: (1) the gain/loss of the photon and (2) the dephasing, with the method in [97], respectively.

As mentioned above, the first pair of excited states can be written by the shifted Fock states  $|\psi_n^\pm\rangle = \mathcal{N}_n^\pm[\hat{D}(\alpha) + (-1)^\pm\hat{D}(-\alpha)]|1\rangle$ . In this approximation, the actions of  $\hat{a}$  and  $\hat{a}^\dagger$  have the following effects:

$$\begin{aligned} \hat{a}|\psi_0^\pm\rangle &= \alpha|\psi_0^\mp\rangle, \\ \hat{a}^\dagger|\psi_0^\pm\rangle &= \alpha|\psi_0^\mp\rangle + |\psi_1^\mp\rangle. \end{aligned} \quad (12)$$

These two operators, corresponding to single-photon loss and thermal photon production process, will cause bit flip and leakage of cat qubit bases, respectively. In Fig. 7(a), we show the fidelity of the NOT gate as functions of  $\kappa_\alpha$  and  $n_{th}$  with  $\Omega = 0.23\text{K}$ , corresponding to  $T_g \approx 27\text{K}^{-1}$ . This result is similar to those of H and A gates, respectively. It can be found that the influences of the thermal photons increases as the rate of single-photon loss increase. In fact, when  $\kappa_\alpha/8\text{K}|\alpha|^2 \ll 1$ , the influences of the single-photon loss cause phase space distortion of cat-qubits  $|\pm\alpha\rangle \rightarrow |\pm\tilde{\alpha}\rangle = |\pm r_0 e^{i\theta_0}\rangle$  [87]:

$$\begin{aligned} r_0 &= \left(\frac{4P^2 - \kappa_\alpha^2/4}{4\text{K}^2}\right)^{1/4}, \\ \tan 2\theta_0 &= \frac{\kappa_\alpha}{\sqrt{16P^2 - \kappa_\alpha^2}}. \end{aligned} \quad (13)$$

The influences of dephasing can be divided into two parts:  $\hat{Z}$ -error and leakage to higher excited states. The first part can be suppressed by large  $|\alpha|^2$ , but the second part is inevitable. As shown in Fig. 7(b), the influences of dephasing are larger than those of single-photon loss due to the leakage to higher excited states. To perform the non-adiabatic holonomic gate, the key is to decrease leakage to higher excited states, which may be solved by combining other technologies, such as derivative-based transition suppression technique [13], to alleviate this noise, or to improve the Kerr nonlinearity K.

Finally, we study the influences of the fluctuation of the amplitudes for both the single- and two-photon drives. The gate's sensitivity to the fluctuations of  $\Omega_s = \Omega c_1'$  and  $\Omega_t = \Omega c_0'$  is shown in Fig. 7(c) with  $\Omega = 0.23\text{K}$ . This result shows that gate fidelity is only reduced by about 1% for 4% of the deviation of  $\Omega_s$  and  $\Omega_t$ , revealing the potential advantage of the gate.

Extension of numerical calculations including decoherence and leakage to the cases of the two-qubit gates is intuitive and similar, results of which are not shown due to the large overhead of our computation capacity at hand.

## VI. DISCUSSION AND OUTLOOK

In conclusion, we have shown that the non-adiabatic holonomic single- and two-qubit operations can be achieved with cat qubits through the KPO and the coupled KPOs with the combination of the single- and two-photon driving processes. Further improved gate fidelities may be reached with the support of the developed optimized methods, such as derivative-based transition suppression techniques [83]. Experimental demonstration of these constructed gates can be expected, attributed to the developments of the single cat qubit gates with a KPO, realized with superconducting circuit systems [97].

## ACKNOWLEDGMENTS

This work was supported by the National Natural Science Foundation of China under Grand Nos. 12274080 and 11875108.

### Appendix A: Non-adiabatic holonomic operation based on cat-qubit

In this section, we derive the realization of non-adiabatic holonomic operations in the KPO system. We consider the method in Ref. [32] and derive this formula from Schrödinger equation. In the rotating frame of  $\hat{H}_{\text{KPO}}$ , due to the parity selectivity of the cat qubit, the Hamiltonian in Eq. (3) can be rewritten as:

$$\begin{aligned} \hat{H}_r &= e^{i\hat{H}_{\text{KPO}}t/\hbar} \hat{H}_{\text{Single}} e^{-i\hat{H}_{\text{KPO}}t/\hbar} \\ &= \frac{\Omega}{2} \left[ c_0 e^{-i\xi} \sum_{i,j=0} \left( \langle \psi_i^+ | \frac{\hat{a}^2}{2} | \psi_j^+ \rangle e^{i\delta_{ij}^{++}t} | \psi_i^+ \rangle \langle \psi_j^+ | + \langle \psi_i^- | \frac{\hat{a}^2}{2} | \psi_j^- \rangle e^{i\delta_{ij}^{--}t} | \psi_i^- \rangle \langle \psi_j^- | \right) + \text{H.c.} \right] \\ &\quad + \frac{\Omega}{2} \left[ c_1 e^{-i\xi} \sum_{i,j=0} \left( \langle \psi_i^+ | \hat{a} | \psi_j^- \rangle e^{i\delta_{ij}^{+-}t} | \psi_i^- \rangle \langle \psi_j^+ | + \langle \psi_i^- | \hat{a} | \psi_j^+ \rangle e^{i\delta_{ij}^{-+}t} | \psi_i^+ \rangle \langle \psi_j^- | \right) + \text{H.c.} \right], \end{aligned} \quad (\text{A1})$$

where  $\delta_{ij}^{+-} = (E_i^+ - E_j^-)/\hbar - \omega$  and  $E_0^+ = E_0^-$ . We control  $\omega = [E_1^+ - E_0^+ (\text{or } E_0^-)]/\hbar$  and  $\Omega \ll |[E_1^- - E_0^+ (\text{or } E_0^-)]/\hbar|$ , and drop the high-frequency oscillation terms according to rotating wave approximation. The Hamiltonian can be simplified as below:

$$\hat{H}'_{\text{Single}} = \frac{\Omega}{2} \left( c'_0 e^{-i\xi} |2\rangle_L \langle 1| + c'_1 e^{-i\xi} |2\rangle_L \langle 0| + \text{H.c.} \right), \quad (\text{A2})$$

where  $c'_0 = c_0 \langle 1|a|2\rangle_L$  and  $c'_1 = c_1 \langle 0|a^2|2\rangle_L/2$ . We encode  $|\psi_0^+\rangle$ ,  $|\psi_0^-\rangle$ , and  $|\psi_1^+\rangle$  as  $|0\rangle_L$ ,  $|1\rangle_L$ , and  $|2\rangle_L$ , respectively. Provided  $\xi = 0$ ,  $c'_0 = \sin(\theta/2)e^{-i\phi}$  and  $c'_1 = \cos(\theta/2)$ , the corresponding dark state of the Hamiltonian in Eq. (A2) is written as  $|D\rangle = -\sin(\theta/2)e^{-i\phi}|0\rangle_L + \cos(\theta/2)|1\rangle_L$ , that remains steady. The unitary operator of the evolution dominated by the Hamiltonian (A2) in the subspace  $\{|D\rangle, |B\rangle, |2\rangle_L\}$  can be modelled as:

$$\hat{U}_{\text{Single}}(T_g, 0) = \begin{pmatrix} 1 & 0 & 0 \\ 0 & \cos(\Omega T_g/2) & -i \sin(\Omega T_g/2) \\ 0 & -i \sin(\Omega T_g/2) & \cos(\Omega T_g/2) \end{pmatrix}, \quad (\text{A3})$$

which reduces to  $\hat{U}_{\text{Single}}(T_g, 0) = -(|2\rangle_L \langle 2| + |B\rangle_L \langle B|) + |D\rangle_L \langle D|$ , with  $T_g = 2\pi/\Omega$ . If the KPO is confined within

the subspace  $\{|0\rangle_L, |1\rangle_L\}$ , the unitary transformation can be described as below:

$$\hat{U}_{\text{Single}}(\theta, \phi) = \begin{pmatrix} \cos \theta & e^{-i\phi} \sin \theta \\ e^{i\phi} \sin \theta & -\cos \theta \end{pmatrix}. \quad (\text{A4})$$

With the choices of  $(\theta, \phi)$  as  $(3\pi/2, 0)$ ,  $(3\pi/2, \pi/4)$  and  $(7\pi/4, 0)$ , we can realize NOT, A, and H gates, respectively, which form a complete set of single-qubit gates.

Two-qubit operations can be done in a similar way. We design the specific coupling mechanism to drive the oscillation between  $|B\rangle$  and  $|2\rangle_L$  of the controlled-KPO when the state of the control-KPO is  $|1\rangle_L$  by the parity selectivity. To alleviate the leakage to the other excited states, we should control the coupling strength much smaller than the gap between the other excited states and the state to be driven. The process can be described as:

$$\hat{U}_{\text{Two}}(\theta, \phi) = \begin{pmatrix} 1 & 0 & 0 & 0 \\ 0 & 1 & 0 & 0 \\ 0 & 0 & \cos \theta & e^{-i\phi} \sin \theta \\ 0 & 0 & e^{i\phi} \sin \theta & -\cos \theta \end{pmatrix}. \quad (\text{A5})$$

[1] M. V. Berry, Quantal phase factors accompanying adiabatic changes, *Proc. R. Soc. Lond. A.* **392**, 45 (1984).

[2] S. Berger, M. Pechal, A. A. Abdumalikov, C. Eichler, L. Steffen, A. Fedorov, A. Wallraff, and S. Filipp, Ex-

- ploring the effect of noise on the berry phase, *Phys. Rev. A* **87**, 060303 (2013).
- [3] G. Falci, R. Fazio, G. M. Palma, J. Siewert, and V. Vedral, Detection of geometric phases in superconducting nanocircuits, *Nature* **407**, 355 (2000).
- [4] S.-L. Zhu and P. Zanardi, Geometric quantum gates that are robust against stochastic control errors, *Phys. Rev. A* **72**, 020301 (2005).
- [5] Y. Y. Huang, Y. K. Wu, F. Wang, P. Y. Hou, W. B. Wang, W. G. Zhang, W. Q. Lian, Y. Q. Liu, H. Y. Wang, H. Y. Zhang, L. He, X. Y. Chang, Y. Xu, and L. M. Duan, Experimental realization of robust geometric quantum gates with solid-state spins, *Phys. Rev. Lett.* **122**, 010503 (2019).
- [6] J. A. Jones, V. Vedral, A. Ekert, and G. Castagnoli, Geometric quantum computation using nuclear magnetic resonance, *Nature* **403**, 869 (2000).
- [7] D. M. Tong, Quantitative condition is necessary in guaranteeing the validity of the adiabatic approximation, *Phys. Rev. Lett.* **104**, 120401 (2010).
- [8] S. Ashhab, J. R. Johansson, and F. Nori, Decoherence in a scalable adiabatic quantum computer, *Phys. Rev. A* **74**, 052330 (2006).
- [9] M. G. Bason, M. Viteau, N. Malossi, P. Huillery, E. Arimondo, D. Ciampini, R. Fazio, V. Giovannetti, R. Manella, and O. Morsch, High-fidelity quantum driving, *Nat. Phys.* **8**, 147 (2012).
- [10] B. Zhou, A. Baksic, H. Ribeiro, C. Yale, F. . Heremans, P. Jerger, A. Auer, G. Burkard, A. Clerk, and D. Awschalom, Accelerated quantum control using superadiabatic dynamics in a solid-state lambda system, *Nat. Phys.* **13**, 330 (2017).
- [11] T. Yan, B.-J. Liu, K. Xu, C. Song, S. Liu, Z. Zhang, H. Deng, Z. Yan, H. Rong, K. Huang, M.-H. Yung, Y. Chen, and D. Yu, Experimental realization of nonadiabatic shortcut to non-abelian geometric gates, *Phys. Rev. Lett.* **122**, 080501 (2019).
- [12] J. Chu, D. Li, X. Yang, S. Song, Z. Han, Z. Yang, Y. Dong, W. Zheng, Z. Wang, X. Yu, D. Lan, X. Tan, and Y. Yu, Realization of superadiabatic two-qubit gates using parametric modulation in superconducting circuits, *Phys. Rev. Appl.* **13**, 064012 (2020).
- [13] F. Motzoi and F. K. Wilhelm, Improving frequency selection of driven pulses using derivative-based transition suppression, *Phys. Rev. A* **88**, 062318 (2013).
- [14] Y. Aharonov and J. Anandan, Phase change during a cyclic quantum evolution, *Phys. Rev. Lett.* **58**, 1593 (1987).
- [15] W. Xiang-Bin and M. Keiji, Nonadiabatic conditional geometric phase shift with NMR, *Phys. Rev. Lett.* **87**, 097901 (2001).
- [16] S.-L. Zhu and Z. D. Wang, Implementation of universal quantum gates based on nonadiabatic geometric phases, *Phys. Rev. Lett.* **89**, 097902 (2002).
- [17] X.-X. Yang, L.-L. Guo, H.-F. Zhang, L. Du, C. Zhang, H.-R. Tao, Y. Chen, P. Duan, Z.-L. Jia, W.-C. Kong, and G.-P. Guo, Experimental implementation of short-path nonadiabatic geometric gates in a superconducting circuit, *Phys. Rev. Appl.* **19**, 044076 (2023).
- [18] D. Leibfried, B. DeMarco, V. Meyer, D. Lucas, M. Barrett, J. Britton, W. M. Itano, B. Jelenkovi, C. Langer, T. Rosenband, and D. J. Wineland, Experimental demonstration of a robust, high-fidelity geometric two ion-qubit phase gate, *Nature* **422**, 412 (2003).
- [19] Y. Xu, Z. Hua, T. Chen, X. Pan, X. Li, J. Han, W. Cai, Y. Ma, H. Wang, Y. . Song, Z.-Y. Xue, and L. Sun, Experimental implementation of universal nonadiabatic geometric quantum gates in a superconducting circuit, *Phys. Rev. Lett.* **124**, 230503 (2020).
- [20] P. Zhao, Z. Dong, Z. Zhang, G. Guo, D. Tong, and Y. Yin, Experimental realization of nonadiabatic geometric gates with a superconducting xmon qubit, *Sci. China Phys. Mech. Astron.* **64**, 250362 (2021).
- [21] C. Song, S.-B. Zheng, P. Zhang, K. Xu, L. Zhang, Q. Guo, W. Liu, D. Xu, H. Deng, K. Huang, D. Zheng, X. Zhu, and H. Wang, Continuous-variable geometric phase and its manipulation for quantum computation in a superconducting circuit, *Nat. Commun.* **8**, 1061 (2017).
- [22] F. Kleiler, A. Lazariiev, and S. Arroyo-Camejo, Universal, high-fidelity quantum gates based on superadiabatic, geometric phases on a solid-state spin-qubit at room temperature, *npj Quantum Inf.* **4**, 49 (2018).
- [23] J. Du, P. Zou, and Z. D. Wang, Experimental implementation of high-fidelity unconventional geometric quantum gates using an nmr interferometer, *Phys. Rev. A* **74**, 020302 (2006).
- [24] H. Imai and A. Morinaga, Demonstration of pure geometric universal single-qubit operation on two-level atoms, *Phys. Rev. A* **78**, 010302 (2008).
- [25] L. Wang, T. Tu, B. Gong, C. Zhou, and G.-C. Guo, Experimental realization of non-adiabatic universal quantum gates using geometric landau-zener-stückelberg interferometry, *Sci. Rep.* **6**, 19048 (2016).
- [26] F. Wilczek and A. Zee, Appearance of gauge structure in simple dynamical systems, *Phys. Rev. Lett.* **52**, 2111 (1984).
- [27] P. Zanardi and M. Rasetti, Holonomic quantum computation, *Phys. Lett. A* **264**, 94 (1999).
- [28] L.-M. Duan, J. I. Cirac, and P. Zoller, Geometric manipulation of trapped ions for quantum computation, *Science* **292**, 1695 (2001).
- [29] K. Toyoda, K. Uchida, A. Noguchi, S. Haze, and S. Urabe, Realization of holonomic single-qubit operations, *Phys. Rev. A* **87**, 052307 (2013).
- [30] F. Leroux, K. Pandey, R. Rehbi, F. Chevy, C. Miniatura, B. Grmaud, and D. Wilkowsky, Non-abelian adiabatic geometric transformations in a cold strontium gas, *Nat. Commun.* **9**, 3580 (2018).
- [31] J. Anandan, Non-adiabatic non-abelian geometric phase, *Phys. Lett. A* **133**, 171 (1988).
- [32] E. Sjöqvist, D. M. Tong, L. Mauritz Andersson, B. Hessmo, M. Johansson, and K. Singh, Non-adiabatic holonomic quantum computation, *New J. Phys.* **14**, 103035 (2012).
- [33] G. F. Xu, J. Zhang, D. M. Tong, E. Sjöqvist, and L. C. Kwek, Nonadiabatic holonomic quantum computation in decoherence-free subspaces, *Phys. Rev. Lett.* **109**, 170501 (2012).
- [34] P. Z. Zhao, G. F. Xu, and D. M. Tong, Advances in nonadiabatic holonomic quantum computation, *Chin. Sci. Bull.* **66**, 1935 (2021).
- [35] J. Zhang, T. H. Kyaw, S. Filipp, L.-C. Kwek, E. Sjöqvist, and D. Tong, Geometric and holonomic quantum computation, *Phys. Rep.* **1027**, 1 (2023).
- [36] Y. Liang, P. Shen, T. Chen, and Z.-Y. Xue, Nonadiabatic holonomic quantum computation and its optimal control, *Sci. Chin. Inf. Sci.* **66**, 180502 (2023).

- [37] G. F. Xu, C. L. Liu, P. Z. Zhao, and D. M. Tong, Nonadiabatic holonomic gates realized by a single-shot implementation, *Phys. Rev. A* **92**, 052302 (2015).
- [38] E. Sjöqvist, Nonadiabatic holonomic single-qubit gates in off-resonant systems, *Phys. Lett. A* **380**, 65 (2016).
- [39] E. Herterich and E. Sjöqvist, Single-loop multiple-pulse nonadiabatic holonomic quantum gates, *Phys. Rev. A* **94**, 052310 (2016).
- [40] G. F. Xu, D. M. Tong, and E. Sjöqvist, Path-shortening realizations of nonadiabatic holonomic gates, *Phys. Rev. A* **98**, 052315 (2018).
- [41] M. E. Tasgin, M. Gunay, and M. S. Zubairy, Nonclassicality and entanglement for wave packets, *Phys. Rev. A* **101**, 062316 (2020).
- [42] G. F. Xu, P. Z. Zhao, T. H. Xing, E. Sjöqvist, and D. M. Tong, Composite nonadiabatic holonomic quantum computation, *Phys. Rev. A* **95**, 032311 (2017).
- [43] N. Ramberg and E. Sjöqvist, Environment-assisted holonomic quantum maps, *Phys. Rev. Lett.* **122**, 140501 (2019).
- [44] F. Zhang, J. Zhang, P. Gao, and G. Long, Searching nonadiabatic holonomic quantum gates via an optimization algorithm, *Phys. Rev. A* **100**, 012329 (2019).
- [45] P. Z. Zhao, G. F. Xu, Q. M. Ding, E. Sjöqvist, and D. M. Tong, Single-shot realization of nonadiabatic holonomic quantum gates in decoherence-free subspaces, *Phys. Rev. A* **95**, 062310 (2017).
- [46] Z.-T. Liang, Y.-X. Du, W. Huang, Z.-Y. Xue, and H. Yan, Nonadiabatic holonomic quantum computation in decoherence-free subspaces with trapped ions, *Phys. Rev. A* **89**, 062312 (2014).
- [47] J. Zhang, L.-C. Kwek, E. Sjöqvist, D. M. Tong, and P. Zanardi, Quantum computation in noiseless subsystems with fast non-abelian holonomies, *Phys. Rev. A* **89**, 042302 (2014).
- [48] P. Z. Zhao, X. Wu, and D. M. Tong, Dynamical-decoupling-protected nonadiabatic holonomic quantum computation, *Phys. Rev. A* **103**, 012205 (2021).
- [49] J. Zhang, S. J. Devitt, J. Q. You, and F. Nori, Holonomic surface codes for fault-tolerant quantum computation, *Phys. Rev. A* **97**, 022335 (2018).
- [50] C. Wu, Y. Wang, X.-L. Feng, and J.-L. Chen, Holonomic quantum computation in surface codes, *Phys. Rev. Appl.* **13**, 014055 (2020).
- [51] A. A. Abdumalikov Jr, J. M. Fink, K. Juliusson, M. Pechal, S. Berger, A. Wallraff, and S. Filipp, Experimental realization of non-abelian non-adiabatic geometric gates, *Nature* **496**, 482 (2013).
- [52] Y. Xu, W. Cai, Y. Ma, X. Mu, L. Hu, T. Chen, H. Wang, Y. Song, Z.-Y. Xue, Z.-q. Yin, and L. Sun, Single-loop realization of arbitrary nonadiabatic holonomic single-qubit quantum gates in a superconducting circuit, *Phys. Rev. Lett.* **121**, 110501 (2018).
- [53] Z. Zhang, P. Z. Zhao, T. Wang, L. Xiang, Z. Jia, P. Duan, D. M. Tong, Y. Yin, and G. Guo, Single-shot realization of nonadiabatic holonomic gates with a superconducting qutrit, *New J. Phys.* **21**, 073024 (2019).
- [54] S. Li, B.-J. Liu, Z. Ni, L. Zhang, Z.-Y. Xue, J. Li, F. Yan, Y. Chen, S. Liu, M.-H. Yung, Y. Xu, and D. Yu, Superrobust geometric control of a superconducting circuit, *Phys. Rev. Appl.* **16**, 064003 (2021).
- [55] D. J. Egger, M. Ganzhorn, G. Salis, A. Fuhrer, P. Müller, P. K. Barkoutsos, N. Moll, I. Tavernelli, and S. Filipp, Entanglement generation in superconducting qubits using holonomic operations, *Phys. Rev. Appl.* **11**, 014017 (2019).
- [56] K. Xu, W. Ning, X.-J. Huang, P.-R. Han, H. Li, Z.-B. Yang, D. Zheng, H. Fan, and S.-B. Zheng, Demonstration of a non-abelian geometric controlled-not gate in a superconducting circuit, *Optica* **8**, 972 (2021).
- [57] S. Danilin, A. Vepsilinen, and G. S. Paraoanu, Experimental state control by fast non-abelian holonomic gates with a superconducting qutrit, *Phys. Scr.* **93**, 055101 (2018).
- [58] Z. Han, Y. Dong, B. Liu, X. Yang, S. Song, L. Qiu, D. Li, J. Chu, W. Zheng, J. Xu, T. Huang, Z. Wang, X. Yu, X. Tan, D. Lan, M.-H. Yung, and Y. Yu, Experimental realization of universal time-optimal non-abelian geometric gates (2020), [arXiv:2004.10364](https://arxiv.org/abs/2004.10364).
- [59] Z. Zhu, T. Chen, X. Yang, J. Bian, Z.-Y. Xue, and X. Peng, Single-loop and composite-loop realization of nonadiabatic holonomic quantum gates in a decoherence-free subspace, *Phys. Rev. Appl.* **12**, 024024 (2019).
- [60] G. Feng, G. Xu, and G. Long, Experimental realization of nonadiabatic holonomic quantum computation, *Phys. Rev. Lett.* **110**, 190501 (2013).
- [61] H. Li, Y. Liu, and G. Long, Experimental realization of single-shot nonadiabatic holonomic gates in nuclear spins, *Sci. China Phys. Mech. Astron.* **60**, 080311 (2017).
- [62] B. B. Zhou, P. C. Jerger, V. Shkolnikov, F. J. Heremans, G. Burkard, and D. D. Awschalom, Holonomic quantum control by coherent optical excitation in diamond, *Phys. Rev. Lett.* **119**, 140503 (2017).
- [63] C. Zu, W. B. Wang, L. He, W. G. Zhang, C. Y. Dai, F. Wang, and L. M. Duan, Experimental realization of universal geometric quantum gates with solid-state spins, *Nature* **514**, 72 (2014).
- [64] S. Arroyo-Camejo, A. Lazarev, S. W. Hell, and G. Balasubramanian, Room temperature high-fidelity holonomic single-qubit gate on a solid-state spin, *Nat. Commun.* **5**, 4870 (2014).
- [65] Y. Sekiguchi, N. Niikura, R. Kuroiwa, H. Kano, and H. Kosaka, Optical holonomic single quantum gates with a geometric spin under a zero field, *Nature Photon.* **11**, 309 (2017).
- [66] K. Nagata, K. Kuramitani, Y. Sekiguchi, and H. Kosaka, Universal holonomic quantum gates over geometric spin qubits with polarised microwaves, *Nat. Commun.* **9**, 3227 (2018).
- [67] N. Ishida, T. Nakamura, T. Tanaka, S. Mishima, H. Kano, R. Kuroiwa, Y. Sekiguchi, and H. Kosaka, Universal holonomic single quantum gates over a geometric spin with phase-modulated polarized light, *Opt. Lett.* **43**, 2380 (2018).
- [68] M.-Z. Ai, S. Li, Z. Hou, R. He, Z.-H. Qian, Z.-Y. Xue, J.-M. Cui, Y.-F. Huang, C.-F. Li, and G.-C. Guo, Experimental realization of nonadiabatic holonomic single-qubit quantum gates with optimal control in a trapped ion, *Phys. Rev. Appl.* **14**, 054062 (2020).
- [69] L. Hu, Y. Ma, W. Cai, X. Mu, Y. Xu, W. Wang, Y. Wu, H. Wang, Y. P. Song, C. L. Zou, S. M. Girvin, L. M. Duan, and L. Sun, Quantum error correction and universal gate set operation on a binomial bosonic logical qubit, *Nat. Phys.* **15**, 503 (2019).
- [70] Y. Ma, Y. Xu, X. Mu, W. Cai, L. Hu, W. Wang, X. Pan,



- H. Wang, Y. P. Song, C. L. Zou, and L. Sun, Error-transparent operations on a logical qubit protected by quantum error correction, *Nat. Phys.* **16**, 827 (2020).
- [71] W. Cai, Y. Ma, W. Wang, C.-L. Zou, and L. Sun, Bosonic quantum error correction codes in superconducting quantum circuits, *Fundam. Res.* **1**, 50 (2021).
- [72] M. H. Michael, M. Silveri, R. . Brierley, V. V. Albert, J. Salmilehto, L. Jiang, and S. . Girvin, New class of quantum error-correcting codes for a bosonic mode, *Phys. Rev. X* **6**, 031006 (2016).
- [73] V. V. Albert, K. Noh, K. Duivenvoorden, D. J. Young, R. T. Brierley, P. Reinhold, C. Vuillot, L. Li, C. Shen, S. M. Girvin, B. M. Terhal, and L. Jiang, Performance and structure of single-mode bosonic codes, *Phys. Rev. A* **97**, 032346 (2018).
- [74] A. L. Grimsmo, J. Combes, and B. Q. Baragiola, Quantum computing with rotation-symmetric bosonic codes, *Phys. Rev. X* **10**, 011058 (2020).
- [75] W.-L. Ma, S. Puri, R. J. Schoelkopf, M. H. Devoret, S. M. Girvin, and L. Jiang, Quantum control of bosonic modes with superconducting circuits, *Sci. Bull.* **66**, 1789 (2021).
- [76] R. W. Heeres, P. Reinhold, N. Ofek, L. Frunzio, L. Jiang, M. H. Devoret, and R. J. Schoelkopf, Implementing a universal gate set on a logical qubit encoded in an oscillator, *Nat. Commun.* **8**, 94 (2017).
- [77] V. V. Albert, S. O. Mundhada, A. Grimm, S. Touzard, M. H. Devoret, and L. Jiang, Pair-cat codes: autonomous error-correction with low-order nonlinearity, *Quantum Sci. Technol.* **4**, 035007 (2019).
- [78] S. E. Nigg, Deterministic hadamard gate for microwave cat-state qubits in circuit qed, *Phys. Rev. A* **89**, 022340 (2014).
- [79] J. Chiaverini, D. Leibfried, T. Schaetz, M. D. Barrett, R. B. Blakestad, J. Britton, W. M. Itano, J. D. Jost, E. Knill, C. Langer, R. Ozeri, and D. J. Wineland, Realization of quantum error correction, *Nature* **432**, 602 (2004).
- [80] O. Oreshkov, T. A. Brun, and D. A. Lidar, Fault-tolerant holonomic quantum computation, *Phys. Rev. Lett.* **102**, 070502 (2009).
- [81] P. Schindler, J. T. Barreiro, T. Monz, V. Nebendahl, D. Nigg, M. Chwalla, M. Hennrich, and R. Blatt, Experimental repetitive quantum error correction, *Science* **332**, 1059 (2011).
- [82] A. G. Fowler, M. Mariantoni, J. M. Martinis, and A. N. Cleland, Surface codes: Towards practical large-scale quantum computation, *Phys. Rev. A* **86**, 032324 (2012).
- [83] Q. Xu, J. K. Iverson, F. G. S. L. Brando, and L. Jiang, Engineering fast bias-preserving gates on stabilized cat qubits, *Phys. Rev. Res.* **4**, 013082 (2022).
- [84] Y.-H. Chen, W. Qin, X. Wang, A. Miranowicz, and F. Nori, Shortcuts to adiabaticity for the quantum rabi model: Efficient generation of giant entangled cat states via parametric amplification, *Phys. Rev. Lett.* **126**, 023602 (2021).
- [85] M. Mirrahimi, Z. Leghtas, V. V. Albert, S. Touzard, R. J. Schoelkopf, L. Jiang, and M. H. Devoret, Dynamically protected cat-qubits: a new paradigm for universal quantum computation, *New J. Phys.* **16**, 045014 (2014).
- [86] C. Chamberland, K. Noh, P. Arrangoiz-Arriola, E. T. Campbell, C. T. Hann, J. Iverson, H. Putterman, T. C. Bohdanowicz, S. T. Flammia, A. Keller, G. Refael, J. Preskill, L. Jiang, A. H. Safavi-Naeini, O. Painter, and F. G. S. L. Brando, Building a fault-tolerant quantum computer using concatenated cat codes, *PRX Quantum* **3**, 010329 (2022).
- [87] S. Puri, S. Boutin, and A. Blais, Engineering the quantum states of light in a kerr-nonlinear resonator by two-photon driving, *npj Quantum Inf.* **3**, 18 (2017).
- [88] V. V. Albert, C. Shu, S. Krastanov, C. Shen, R.-B. Liu, Z.-B. Yang, R. J. Schoelkopf, M. Mirrahimi, M. H. Devoret, and L. Jiang, Holonomic quantum control with continuous variable systems, *Phys. Rev. Lett.* **116**, 140502 (2016).
- [89] Z. Leghtas, S. Touzard, I. M. Pop, A. Kou, B. Vlastakis, A. Petrenko, K. M. Sliwa, A. Narla, S. Shankar, M. J. Hatridge, M. Reagor, L. Frunzio, R. J. Schoelkopf, M. Mirrahimi, and M. H. Devoret, Confining the state of light to a quantum manifold by engineered two-photon loss, *Science* **347**, 853 (2015).
- [90] M. Mirrahimi, Cat-qubits for quantum computation, *C. R. Phys.* **17**, 778 (2016).
- [91] J.-J. Xue, K.-H. Yu, W.-X. Liu, X. Wang, and H.-R. Li, Fast generation of cat states in kerr nonlinear resonators via optimal adiabatic control, *New J. Phys.* **24**, 053015 (2022).
- [92] B. Yurke and D. Stoler, The dynamic generation of schrödinger cats and their detection, *Physica B+C* **151**, 298 (1988).
- [93] J. Guillaud and M. Mirrahimi, Repetition cat qubits for fault-tolerant quantum computation, *Phys. Rev. X* **9**, 041053 (2019).
- [94] R. Lescanne, M. Villiers, T. Peronin, A. Sarlette, M. Delbecq, B. Huard, T. Kontos, M. Mirrahimi, and Z. Leghtas, Exponential suppression of bit-flips in a qubit encoded in an oscillator, *Nat. Phys.* **16**, 509 (2020).
- [95] T. Kanao, S. Masuda, S. Kawabata, and H. Goto, Quantum gate for a kerr nonlinear parametric oscillator using effective excited states, *Phys. Rev. Appl.* **18**, 014019 (2022).
- [96] H. Goto, Universal quantum computation with a nonlinear oscillator network, *Phys. Rev. A* **93**, 050301 (2016).
- [97] A. Grimm, N. E. Frattini, S. Puri, S. O. Mundhada, S. Touzard, M. Mirrahimi, S. M. Girvin, S. Shankar, and M. H. Devoret, Stabilization and operation of a kerr-cat qubit, *Nature* **584**, 205 (2020).
- [98] S. Touzard, A. Grimm, Z. Leghtas, S. O. Mundhada, P. Reinhold, C. Axline, M. Reagor, K. Chou, J. Blumoff, K. M. Sliwa, S. Shankar, L. Frunzio, R. J. Schoelkopf, M. Mirrahimi, and M. H. Devoret, Coherent oscillations inside a quantum manifold stabilized by dissipation, *Phys. Rev. X* **8**, 021005 (2018).
- [99] Y.-H. Kang, Y.-H. Chen, X. Wang, J. Song, Y. Xia, A. Miranowicz, S.-B. Zheng, and F. Nori, Nonadiabatic geometric quantum computation with cat-state qubits via invariant-based reverse engineering, *Phys. Rev. Res.* **4**, 013233 (2022).
- [100] Y.-H. Kang, Y. Xiao, Z.-C. Shi, Y. Wang, J.-Q. Yang, J. Song, and Y. Xia, Effective implementation of nonadiabatic geometric quantum gates of cat-state qubits using an auxiliary qutrit, *New J. Phys.* **25**, 033029 (2023).
- [101] Z. Wang, M. Pechal, E. A. Wollack, P. Arrangoiz-Arriola, M. Gao, N. R. Lee, and A. H. Safavi-Naeini, Quantum dynamics of a few-photon parametric oscillator, *Phys. Rev. X* **9**, 021049 (2019).
- [102] W. Ning, X.-J. Huang, P.-R. Han, H. Li, H. Deng, Z.-B.

Yang, Z.-R. Zhong, Y. Xia, K. Xu, D. Zheng, *et al.*, Deterministic entanglement swapping in a superconducting circuit, *Phys. Rev. Lett.* **123**, 060502 (2019).

[103] P. Z. Crispin Gardiner, *Quantum noise* (Springer Berlin, Heidelberg, 2004).